Composites Science and Technology 222 (2022) 109369

Contents lists available at ScienceDirect

Composites Science and Technology

journal homepage: www.elsevier.com/locate/compscitech

Hierarchical carbon fibre composites incorporating high loadings of carbon nanotubes

Neptun Yousefi [a], Sandra J. Fisher [b], Christoph Burgstaller [c], Milo S.P. Shaffer [b], Alexander Bismarck [a,d,*]

[a] Polymer and Composite Engineering (PaCE) Group, Institute of Materials Chemistry, Faculty of Chemistry, University of Vienna, Währinger Straße 42, A-1090, Vienna, Austria
[b] Department of Chemistry, Imperial College London, South Kensington, London, SW7 2AZ, UK
[c] Transfercenter für Kunststofftechnik (TCKT), Franz-Fritsch-Straße 11, A-4600, Wels, Austria
[d] Department of Chemical Engineering, Imperial College London, South Kensington, London, SW7 2AZ, UK

ARTICLE INFO

Keywords:
A. Carbon nanotubes
A. Carbon fibres
B. Mechanical properties
E. Powder processing

ABSTRACT

Uncured solid bisphenol-A epoxy resins containing up to 20 wt% carbon nanotubes (CNTs) were prepared using melt blending in a high shear mixer. The extrudate was ground to produce fine nanocomposite (NC) powders. This simple method produced well-dispersed NC, with CNT agglomerate sizes below 1 μm. Consolidated NCs displayed improved tensile moduli and strengths up to 3.3 GPa (+32%) and 78 MPa (+19%), respectively at 15 wt% CNT, compared to the pure cured epoxy matrix. The relatively high T_g of 39 °C for the uncured NC powders simplified the manufacture of composite prepregs using wet powder impregnation. The prepregs were laminated into hierarchical carbon fibre reinforced composites with improved through-thickness properties. Interlaminar shear strength improved for intermediate CNT loadings in the matrix up to 65 MPa (10 wt% CNT, +19%) but decreased at higher concentrations. Compression moduli remained constant irrespectively of CNT loading but compression strength increased with a CNT loading of 2.5 wt% to 772 MPa (+31%). The mechanical properties of the hierarchical composites reflect good consolidation (void content <3%) and excellent fibre alignment (<±0.8°). In addition to the improved mechanical properties, incorporation of CNTs improved the through-thickness electrical conductivity up to 115 S/m.

1. Introduction

Continuous or long fibre reinforced polymers find widespread application for their excellent specific properties [1]. Their compression performance is often limiting due to premature failure initiated by kink band formation or "microbuckling" of the fibres. One route to improve the out-of-plane properties is to increase the stiffness of the matrix; however, using conventional cross-linked resin systems, the resulting loss of toughness is unacceptable. Instead, there has been widespread interest in using nanofilled or nanostructured matrix systems to improve stiffness and toughness, simultaneously [2]. Examples include dispersing of carbon nanotubes (CNTs), copper oxide [3–5] or silica [6,7] into the matrix system [8,9]. The combination of a nanoscale filler, with conventional microscale fibres, is often termed "hierarchical composite", and analogies are drawn to natural systems, such as wood or bone [9,10]. The use of CNTs as a reinforcement in polymers is attractive for their excellent intrinsic mechanical, electrical and thermal properties [11,12]. However, one key challenge is the homogeneous dispersion of CNTs within the polymer matrix, particularly at higher loadings, due to their high aspect ratio, small size, and strong inter-particle interactions [13]. CNT dispersion is often attempted using ultrasonification, calendering (three roll mills) [14], ball milling, and stirring as well as extrusion [13]. The choice of dispersion method is dependent on the viscosity [13], loading fraction [15], and extent of CNT damage that can be tolerated [16]. In any case, well dispersed nanoparticles are crucial for the mechanical properties of hierarchical composites [17]. Nanocomposites with low loadings (<~1 wt%) of both single walled carbon nanotubes (SWCNTs) or multi-walled carbon nanotubes (MWCNTs) in epoxy resins can increase Young's modulus (intensively shown in Ref. [18]) and show an increase in tensile strength of 4–25% [19]. Strain

* Corresponding author. Polymer and Composite Engineering (PaCE) Group, Institute of Materials Chemistry, Faculty of Chemistry, University of Vienna, Währinger Straße 42, A-1090, Vienna, Austria.
E-mail address: alexander.bismarck@univie.ac.at (A. Bismarck).

https://doi.org/10.1016/j.compscitech.2022.109369
Received 4 December 2021; Received in revised form 18 February 2022; Accepted 26 February 2022
Available online 3 March 2022
0266-3538/© 2022 The Authors. Published by Elsevier Ltd. This is an open access article under the CC BY license (http://creativecommons.org/licenses/by/4.0/).

to failure is typically reduced, however, there are examples where toughness (work of fracture) is increased by around 10% [13,18]. Higher CNT loadings should, in principle, provide improved nanocomposite performance if dispersion can be maintained; higher absolute stiffnesses are particularly important to maximise the constraint of the primary reinforcement in hierarchical fibre reinforced polymer (FRP) composites. Several studies of hierarchical composites with CNT reinforcement in the matrix have shown an improvement in interlaminate shear strength (ILSS) of 8–30% [9]. Fundamentally, improving matrix-dominated properties, such as ILSS, is challenging as both the bulk matrix characteristics and the fibre-matrix interface need to be considered [20]. More practically, manufacturing high CNT loading hierarchical composites is difficult due to the high viscosity of CNT-loaded polymers/resins [21] and the self-filtration of CNTs on carbon fibre (CF) preforms; the problems are exacerbated at higher loadings as the CNTs become increasingly entangled and/or agglomerated. Fabrication methods involving infusion can result in both porosity and CNT concentration gradients that reduce composite performance. For these reasons, most CNT hierarchical composites have low nanofiller loadings, less than 5 wt%, and usually less than 2 wt% [22]. One strategy to increase CNT concentration in the matrix relied on spreading the CF tow in a highly loaded (10 wt%) cup-stacked carbon nanofibre filled resin, followed by filament winding [23]; this approach improved compression modulus (+5%) and strength (+10%) in the fibre direction. The highest CNT loadings (20 wt% resin) in continuous CF epoxy composites reported so far were processed using a powder pregging method [24–26]. However, these previous experiments [24–26] showed relatively poor fibre alignment making it difficult to prepare UD laminates for effective compression tests. Very high viscosities, similar to thermoplastics, are obtained when processing resin systems containing high CNT loadings. Therefore, thermoplastic composite manufacturing methods, e.g. powder pregging, show great promise. Powder pregging mitigates the conventional difficulties of flow or filtration effects during manufacture. Highly CNT loaded thermosetting resins can be produced by shear-mixing (using measuring mixers) blending an epoxy resin and hardener at elevated temperatures. The main requirement is the formation of a powder, while ensuring that no curing occurs during blending. A solid powder is needed during the powder pregging process to avoid premature particle coalescence; many resins have a glass transition temperature (T_g) below or near room temperature before curing, making handling difficult. In this work, we formulated a CNT-epoxy resin with a high uncured T_g (39 °C), which increased pot life and allowed for preparation of uncured nanocomposite powders by simple grinding rather than cryogenic milling. A well-dispersed CNT-in-epoxy resin powder with a small CNT agglomerate size was obtained. The resin powder was characterised prior to nanocomposite (NC) formation and was used to produce hierarchical composites (HC) in combination with carbon fibre tows. The mechanical properties of NC were characterised to determine the best matrices for HC preparation. As already noted, conventional composite manufacturing techniques, such as vacuum-assisted resin transfer moulding (VARTM), are not suitable for highly viscous resin systems. Therefore, a wet-powder impregnation process was used to produce HC prepregs, which were then consolidated using a simple bag press method. The matrix-dominated mechanical properties of the HCs were examined under compression and in shear to assess the effect of high CNT loading. Since the addition of CNTs can benefit other functional properties, particularly electrical conductivity, the generally low transverse conductivities of the composites were monitored.

2. Experimental

2.1. Materials

The matrix comprises of a solid bisphenol-A epoxy resin (Araldite GT7071), which was generously supplied by Huntsman (Duxford, UK). A powdered hardener dicyandiamide (DICY, Dyhard 100 S) supplied by AlzChem (Trostberg, Germany) was used to cure the solid epoxy resin. Multiwalled CNTs (Graphistrength® C100) were supplied by Arkema (France) and epoxy sized polyacrylonitrile-based standard modulus carbon fibres (SIGRAFIL, C T50–4.0/240-E100) containing 50 k filaments were purchased from SGL Carbon (Meitingen, Germany). Composite microsections were prepared using EpoxiCure 2 resin (Buehler, Düsseldorf, Germany). The surfactant 2-[4-(2,4,4-trimethylpentan-2-yl) phenoxy] ethanol, commercially available as Triton X - 100, was used to stabilise the resin suspension in an aqueous impregnation bath, was purchased from Sigma-Aldrich. For composite manufacturing, release agent (Frekote 700-NC) was supplied by Henkel (Germany), polyimide release film (Upilex-25 S) by UBE (Osaka, Japan), vacuum tape (Airdam 1) by Airtech (Luxembourg), and vacuum bag (VB200 Vacuum Bagging Film LFT (1520 mm)) by Easycomposites (UK).

2.2. Solid epoxy resin formulations

Araldite GT7071 epoxy, 5 wt% dicyandiamide hardener (DICY) and varying CNT amounts (0, 2.5, 5, 10, 15 and 20 wt%) were pre-mixed by hand in a sealed container at room temperature. The premixed resin was blended at 55 °C and 53 rpm for 15 min using a measuring mixer (Plastograph, Brabender, Duisburg, Germany; equipped with a 3-zone W50EHT mixing unit). The measuring mixer consists of a temperature-controlled chamber equipped with two blending screws. The mixing head was air cooled during the whole process to compensate for shear heating and thus avoid curing of the resin. The extrudate was collected and then milled into a fine powder using a mechanical grinder (Karcher UM 620). To obtain a uniform particle size, the resin powders were sieved (mesh 40; aperture size 425 μm, Retsch) and subsequently stored in a fridge at 5 °C prior to use.

2.3. Characterisation of uncured solid epoxy resin powders

The particle size of the uncured and sieved epoxy resin powders was determined using laser diffraction (HELOS equipped with a RODOS/M dispersion unit Sympatec, Clausthal-Zellerfeld, Germany). Thermal properties and curing behaviour were characterised using differential scanning calorimetry (DSC) (TA Instruments, Eschborn, Germany). All specimens were heated from 0 °C to 300 °C, cooled back to 0 °C and then re-heated to 300 °C at a rate of 5 °C/min in a nitrogen atmosphere. The density of the uncured resin powders (~9 mg samples) was analysed using helium displacement pycnometry (AccuPyc II 1350, Micrometrics Aachen, Germany). The dispersion of the CNTs within the epoxy resin was determined by optical microscopy. The sample preparation was performed in accordance with Fisher et al. [27]: Briefly, the uncured solid epoxy resin powders were mixed with a clear potting resin (Durcupan ACM, M epoxy resin and hardener 964, Merck) to suspend the powder evenly. This mixture was cured into a block of resin. The resin block was microtomed into thin slices and examined in transmission light microscopy. CNT agglomerate size was measured using ImageJ [28]. The CNT length after mixing uncured NC was determined by dissolving the resin in dimethylformamide (DMF), subsequently the CNT suspension was filtered over a chitin-glucan nanopaper [29], followed by washing the filtrate several times with acetone. The CNTs were imaged in a SEM (Zeiss Supra 55 VP) and the length was measured using ImageJ.

2.4. Nanocomposite preparation

The solid epoxy powders were consolidated into dog bone shaped specimens (ASTM D638 Type V) using a bag pressing method. The mould was covered with peel ply (release fabric, FF03PM, Cytec Engineered Materials Ltd. Wrexham, UK), then filled with solid epoxy resin powders and placed on a metal plate covered with polyimide release film. Around the edge of the mould vacuum bag sealant tape was placed

and another release film placed on top of the mould. The vacuum bagging film was pressed against the sealant tape to create a seal around the mould and a vacuum inlet was placed close to the mould. Vacuum was applied for 15 min at room temperature. The mould was then placed inside a hot press (Model 4126 Manual, Hydraulic Press, Carver, USA), which was pre-heated to 30 °C and vacuuming continued for 30 min at 30 °C. The plates of the hot press were touching the mould but no pressure was applied during the whole procedure. Afterwards, the temperature of the hot press was raised to 150 °C. When the temperature reached approximately 80 °C vacuuming was stopped. The resin was cured at 150 °C for 8 h. The control samples (containing no CNTs) were produced using the same procedure. All specimens were post-cured at 210 °C for 1 h. To remove surface imperfections, the dog bone tensile specimens were polished using a fine sandpaper (P120).

2.5. Characterisation of CNT nanocomposites

Tensile tests were performed following ASTM D636 using a universal dual column testing frame (Series 5969, Instron Ltd., Norwood, UK) equipped with a 50 kN load cell. The strain was recorded using a video extensometer (IMT-CAMO018, camera: GigE PoE, IMETRUM, UK) tracking white (samples containing CNT) or black (control samples without CNT) dots, which were painted onto the NC using opaque white or a black permanent marker, respectively. The testing rate was 0.5 mm/min. The envelope (ρ_e) and skeletal (ρ_s) densities, as well as the voidage (V_v), of the NCs were measured using pycnometry (AccuPyc II 1350 and GeoPyc 1360, Micrometrics Aachen, Germany), on specimens cut from the end tab region of tensile test specimens. The weight was determined using an analytical balance (Sartorius Cubis™ Series, model MSA225P, Göttingen, Germany). The AccuPyc uses He as the fluid to determine the skeletal density, while the GeoPyc uses beads to determine envelope density; the ratio indicates the voidage.

2.6. Manufacturing of hierarchical composites

Continuous pre-impregnated unidirectional carbon fibre reinforced epoxy tapes were manufactured using our bespoke continuous powder impregnation line [26] (Fig. 1). A 50 k carbon fibre roving was fixed into the creel (unit 1) and a pre-tension of 0.5 N was applied (unit 2). Units 1 and 2 together form a creel with tension control (Izumi International, Greenville, SC, USA). The fibre tow was then passed through a custom-made impregnation bath (unit 3) containing 2.5 L suspension with a consistency of 1.5 wt% solid epoxy resin, which was agitated using two 60 mm magnetic stirrer bars. The impregnation bath contains five spreading pins. The wet resin-impregnated fibre tow was then passed through two drying ovens (units 4 & 5) equipped with infrared heaters (Model B, fast response medium wave emitters, Heraeus, Kleinostheim, Germany). The ovens were kept at 120 °C and 135 °C, respectively. The power output for both drying ovens was controlled independently using programmable logic controllers (3508 Eurotherm PID temperature controllers, UK). The fibres were almost completely dried during this stage. The tape emerging from the ovens was passed over three shear impregnation pins (unit 6) heated to 125 °C. The tension generated by the wrap angle of the heated pins spreads the fibres further, driving the polymer into the tow and eliminating voids. Any fibre 'fuzzes' produced during manufacturing were also to be collected here. The uncured composite tape was pulled through the composite line using a belt-driven haul-off device (Model 110–3, RDN Manufacturing Co., Bloomingdale, IL, USA), which was used to control the processing speed (0.25 m/min). The produced uncured HC tapes were cut into 200 mm long sections and weighed. The tape weight was used to control the fibre volume fraction in the composite by adding concentrated uncured resin powder suspension (with 18 wt%) into the impregnation bath.

2.7. Lay-up, consolidation and sample preparation

The prepreg tapes were further dried overnight at room temperature. Compression test specimens were prepared by cutting the tapes into 190 mm long sections, which were then stacked within a stainless-steel mould (200 mm × 12 mm). Two 2 mm thick spacers (5 mm long, 12 mm wide) were also placed at either end of the mould. The mould containing the tapes was then placed within a vacuum bag and degassed for 30 min before being placed into a hot press (Model 4126, Hydraulic Press, Carver, USA). The specimens were heated at 5 °C/min to 50 °C and held at this temperature for 30 min. After this time, a pressing force of 2 t was applied for a further 30 min, while keeping the temperature at 50 °C. Afterwards, the temperature was increased to 150 °C. The vacuum pump was switched off and the specimens cured at 150 °C for 8 h. All specimens were post cured at 210 °C for 1 h. Specimens were removed from the mould at ambient temperature. A diamond blade cutter (Mutronic, Diadisc 4200) was used to cut test specimens to the required dimensions. Compression test specimens (110 mm × 10 mm x 2 mm) were first grit blasted and then cleaned. Four end tab sections (50 mm × 10 mm) with inverse chamfers were glued onto the grit blasted composite surface using epoxy glue (Araldite 2011, Huntsman). To ensure a constant gauge length of 10 mm during curing, a silicone rubber shim was placed along the length of the gauge area. After curing at room temperature for 24 h, strain gauges (LY71, HBM) were glued to both sides of the composite at the centre of the gauge length using an adhesive (Z70, HBM). Compression tests were performed in accordance with the standard EN ISO 14126:2003 using a universal testing machine (Zwick/Roell Z150 (150 kN)). Interlaminar shear strength (ILSS) test specimens were prepared by cutting the composite prepregs into 125 mm long sections, which were then stacked in a stainless-steel mould (125 mm × 20 mm). 4 mm thick spacers were also placed at either end of the mould. The same curing procedure was used as for the preparation of the compression test specimens. ILSS tests were performed following the standard ASTM D 2344/D 2344 M using a universal testing machine equipped with a 50 kN load cell. The span-to-thickness ratio was 4:1 and the test speed 1 mm/min.

2.8. Chemical and physical characterisation of HCs

The fibre volume (V_f) and void volume fraction (V_V) of the hierarchical composites were determined following ASTM D3171. After compression tests were performed, the end tab sections of HC samples were cut (10 mm × 5 mm x 2 mm) and polished to roughen the surface of the HC. Silver paste (Leitsilber, Christine Gröpl, Austria) was applied to

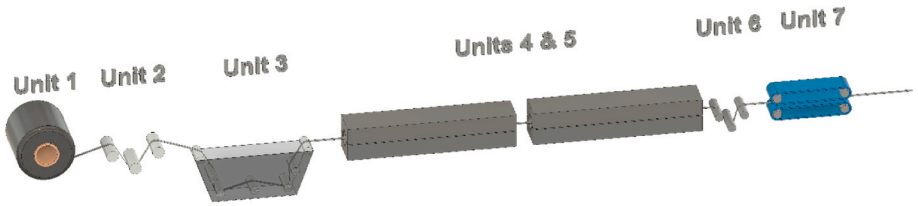


Fig. 1. Schematic of our modular laboratory scale wet powder impregnation composite production line: creel (units 1 & 2), impregnation bath (unit 3), drying ovens (units 4 & 5), shear pin spreading (unit 6) and haul off device (unit 7).

the surface before measuring the electrical conductivity. The electrical conductivity of the HCs was determined using a potentiostat (Gamry Instruments Reference 600) at frequency of 100–100000 Hz and an AC voltage of 10 mV rms. This way a frequency vs resistance curve was generated, where a simplex fit (Gamry Software) was applied to obtain the electrical resistivity.

3. Results and discussion

The solid epoxy resin system (epoxy Araldite GT7071 with 5 wt% DICY) was chosen due to its comparable mechanical properties, once cured, to conventional liquid resin systems [30,31] and for its relatively high uncured T_g, which allows for simple powder processing at room temperature. The CNT-loaded resin blend was ground to form powders, ideally with similar but slightly larger diameters than the CFs (7 μm) to facilitate particle trapping. The particle size d_{SMD} of the resin powders after milling and sieving was on average 13 ± 1 μm (full distributions, ESI Table S1). Following sieving, a rather uniform average particle size was obtained.

The glass transitions temperatures (T_g) measured by DSC (Table 1 and ESI Fig. S1) were consistently around 39 °C and 112 °C for all uncured and cured resin systems, respectively. The addition of CNTs does not influence the T_g significantly; there may be a slight increase after curing, by around 2 °C, consistent with the constraint of the polymer observed in other systems [32], but the effect is small compared to the scatter. The highest curing enthalpy (ΔH_c) was found for the pure resin formulation. ΔH_c decreased proportionally with CNT content, indicating that CNTs did not affect resin stoichiometry, unlike in other reports [33,34]. In our case, the decreasing curing enthalpy is caused by replacing resin with unreactive CNTs. The skeletal densities of the nanocomposite resins (ESI Table S2) after curing followed the linear rule of mixture, assuming a CNT skeletal density of 1791 kg/m^3 (ESI Fig. S2) [35], i.e. the resin density increased linearly from 1192 kg/m^3 with increasing CNT loading. A well-dispersed nanocomposite was achieved by melt blending in a measuring mixer, as judged by optical microscopy sections [27] (Fig. 2). The grey areas indicate a good dispersion, which can be found throughout all resin formulations containing increasing CNT loadings. Only very small black particulates (0.7 μm) suggest CNT agglomeration, which are much shorter than CNT length. Images of all dispersions as well as average agglomeration size of resins containing CNTs (except for 20 wt%) are provided in ESI (ESI Table S3 and Fig. S3).

Nanocomposite powders were consolidated to form dense tensile specimens, which were post-cured at 210 °C to ensure full curing. The resin viscosity increases with CNT loading (from 0 to 15 wt%), as indicated by the increased mixing torque (ESI Fig. S3) resulting in higher shear, shortening the CNTs (example CNT length distributions for 2.5 wt % and 15 wt% CNT samples are shown in ESI Fig. S6). The increased viscosity also complicated specimen degassing during composite preparation, which in turn, resulted in higher void contents at higher CNT loadings as compared to the control resin (ESI Table S4). SEM images of NCs (ESI Figs. S8 and S9) confirm measured void content. The tensile

Table 1
CNT content [CNT] of solid epoxy resins and un/cured glass transition temperature T_g, enthalpy of curing ΔH_c and onset curing temperature T_{on} measured from at least 5 samples.

[CNT] [wt. %]	Uncured T_g[a] [°C]	Cured T_g[a] [°C]	ΔH_c [J/g][b]	T_{on} [°C]
0	38.5 ± 1.1	111.9 ± 2.4	184.6 ± 3.7	174.9 ± 1.7
2.5	38.0 ± 0.8	111.1 ± 1.8	178.1 ± 9.0	184.1 ± 3.3
5	38.9 ± 0.8	113.2 ± 2.0	171.4 ± 1.2	183.1 ± 1.0
10	39.0 ± 1.3	113.5 ± 2.2	164.7 ± 1.2	182.7 ± 2.4
15	40.2 ± 1.8	114.0 ± 0.9	145.5 ± 6.6	181.9 ± 1.2
20	41.6 ± 1.8	113.8 ± 0.9	129.9 ± 0.8	180.7 ± 0.1

[a] Determined by DSC.
[b] Per gram nanocomposite.

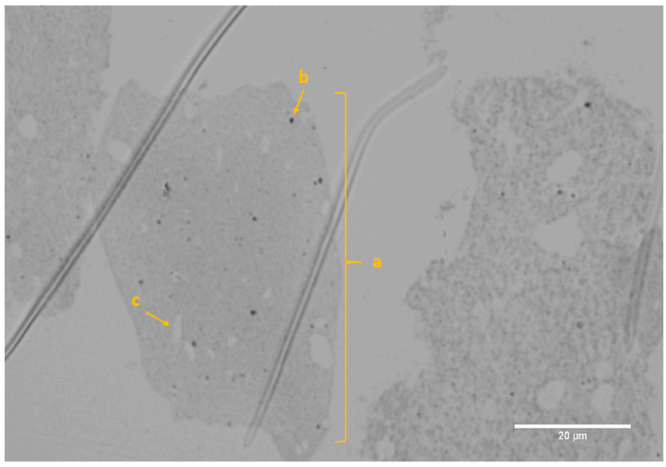


Fig. 2. Characteristic optical micrograph of a microtomed solid resin dispersion containing 10 wt% CNTs. The (a) nanocomposite powder particle, (b) CNT agglomerations and (c) DICY hardener particle inclusions are highlighted.

moduli (E_t) and tensile strengths (σ_t) of the nanocomposites increased with CNT loadings up to 15 wt% (Fig. 3), reaching 3.3 GPa (+32%) and 78 MPa (+19%), respectively (percentage relative to the pure cured epoxy matrix). At 20 wt% CNT loading, the strength and stiffness decreased significantly due to much higher voidage (27 ± 2%).

Herceg et al. [36] found a similar trend for the tensile properties of CNT epoxy composites, however, they reached higher absolute moduli (~5.25 GPa) and strengths (~90 MPa), probably due to the different CNTs used (Nanocyl, NC7000) and lower voidage of their NCs. Due to the voidage it was necessary to correct the measured elastic moduli. The measured elastic moduli E_{NC} for pure matrix and NCs were corrected for the void content using Equation (1) [37], which was substituted into Equation (2) for E_m. The raw CNT weight fraction was also corrected for the remaining growth catalyst and support (7 wt% Al_2O_3 and iron oxide) as determined gravimetrically.

$$E_{resin} = E_{NC}\left(\frac{\rho_s}{\rho_e}\right)^2 \quad (1)$$

The Krenchel equation [38] is often applied to predict the elastic moduli (E) of nanocomposites, adjusting a simple rule of mixtures with efficiency factors for length (η_l) and orientation (η_o) (Equation (2)):

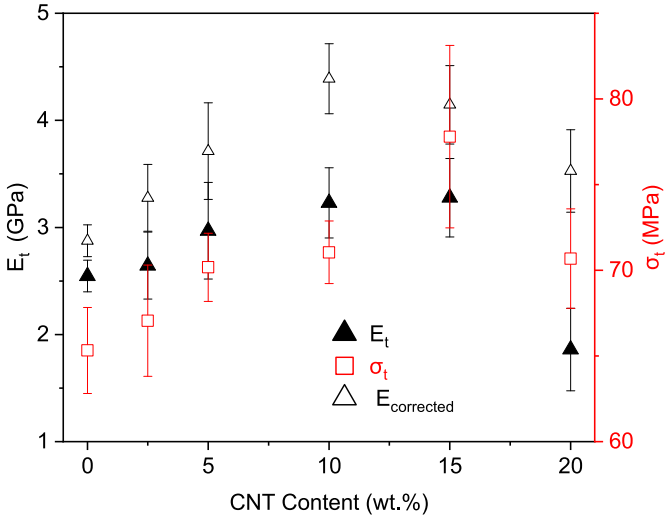


Fig. 3. Measured tensile moduli (E_t) and those corrected for voidage ($E_{corrected}$) and measured strengths (σ_t) of CNT nanocomposites.

$$E = \eta_o \bullet \eta_l \bullet V_f \bullet E_f + (1 - V_f) \bullet E_m \quad (2)$$

where V_f is the CNT volume fraction, E_m the measured matrix modulus, E_f the CNT modulus. Due to the similar CNT lengths distributions, we used $\eta_l = 0.186$ and $\eta_o = 0.375$, the value for an anisotropic fibre (CNT) network, as reported by Herceg et al. [36]. Fitting the determined elastic moduli of the nanocomposites, predicts the modulus of the CNTs to be 66.3 ± 5.3 GPa. This value is in line with many reported in the literature for defective, bulk, CVD CNTs [36,39,40], although significantly lower than expected for perfect, crystalline materials. Many studies on thermoset CNT nanocomposites have shown moderately or significantly increased Young's moduli, often with a more limited increase or even a decrease in strength and toughness [18]. Considering the improved NC properties obtained at higher CNT loading, here, hierarchical composites were prepared using these NC matrices.

UD hierarchical composite prepregs with an average fibre volume fraction of 57% were produced using our wet-powder impregnation process. Additional information on the actual volume fraction and void content of each composite specimen used for ILSS tests is given in ESI (ESI Table S5). The ILSS was assessed using short beam shear (SBS) tests.

ILSS increased with increasing CNT content (Fig. 4A), reaching a maximum of 65 MPa (19% increase) for HCs containing 10 wt% CNTs. However, when increasing the amount of CNTs further (≥15 wt%), a significant decrease in ILSS was observed, which was caused by the higher void fractions of the composites (Fig. 4B). Since the resin and fibre surface chemistry remains unchanged, the interfacial adhesion should also remain unaffected; therefore, the improved ILSS can be attributed to the improved mechanical properties of the matrix [41]. The greater improvement in ILSS, here, at 10 wt% CNTs, compared to Herceg et al. [24], may be due to the lower void content (1.2 ± 0.6% compared to 2.5 ± 1.7%).

Compression properties are generally matrix-dominated but often difficult to improve. The compression moduli (E_c) and strengths (σ_c) of the hierarchical composites (Fig. 5A and B) were tested for HC with CNT loadings up to 15 wt%.

The carbon fibre manufacturer states a compression modulus of 125 GPa for typical epoxy composites normalised to a fibre volume fraction of 60% [42]. The values measured here are in good agreement, indicating an excellent fibre alignment, which was indeed determined (in accordance to Yurgartis [43]) to be within 1° of the main composite axis (ESI Fig. S7 and ESI Table S6). The void content of the compression HC specimens was around 2 ± 1% (ESI Table S7). The compression moduli of all (HC) composites, which are dominated by carbon fibre properties, were on average 118 GPa. HC containing 2.5 wt% CNT provided the greatest increase in compression strength, reaching 772 MPa (+31% over the control composite (0 wt% CNT)). This increase in compression strength, observed for composites containing 2.5 wt% CNTs, is in line with other reports using particulate nanomaterials, such as nanographite and alumina, as matrix reinforcements. However, previous studies only achieved a 3% increase of the compression strength [44–46]. The increased compression strength indicates improved lateral support of the carbon fibres in the hierarchical composites caused by the improved mechanical properties of the CNT enhanced resin system (Fig. 3). Despite reported manufacturer data, our control HC composites (0 wt% CNT) showed comparable compressive strength to UD composites comprising T700 and T800 carbon fibres and an epoxy resin [47].

The fractographic assessment of compression failure is often complex because surface debris originating from the fracture can mask many fractographic aspects (see Fig. 6). During compression loading, the polymer matrix transfers stress to and supports the fibre, which ultimately delays microbuckling [48]. In the HC composites, microbuckling is delayed further by the incorporation CNTs in the matrix, resulting in improved matrix strengths and moduli (Fig. 3) translating to improved HC compression properties. Fig. 6 (2.5–15 wt% CNT) shows terraces that are very characteristic for fibre failure caused by microbuckling and kink band formation. Bands of fibres failed at identical lengths (ranging between 30 and 45 μm), reflecting either low matrix stiffness or crack propagation along the fibre-matrix interface [49]. Here, cracks propagated along the fibre-matrix interface (ESI Fig. S10 #32/33, for 15 wt %). Interestingly, it seems that the fibres were much better supported by the matrix reinforced with 2.5 wt% CNTs, resulting in an additional kink band fracture (ESI Fig. S10 #9–11 for 2.5 wt% CNT & S10 #20–22 for 10 wt% CNT). Secondary damage, such as delamination, was also observed since the compression fracture surfaces still carry load after failure (0, 10 and 15 wt% CNT composites). This observation implies that the microbuckling process that leads to kink band formation is affected by the occurrence of interfacial cracks, as proposed by Argon [50]. For HCs containing 5, 10 and 15 wt% CNTs, the fibre failure occurred predominantly by microbuckling and kink band formation but the fracture surface was partially covered by debris and showed delamination failure, which is reflected in relatively poor compression properties.

The through-thickness electrical conductivity of HCs may be important for lighting strike protection [51], electrostatic discharge (ESD) and electromagnetic interference (EMI) shielding applications [52]. The through-thickness electrical conductivity of unidirectional fibre reinforced composites is usually very low (10^{-3}-10^{-1} S/m) [53–55] compared to their in-plane conductivity (10^4 S/m) [56]. In our experiments, the through-thickness conductivities were relatively high (Fig. 7) due to the compression applied during sample consolidation

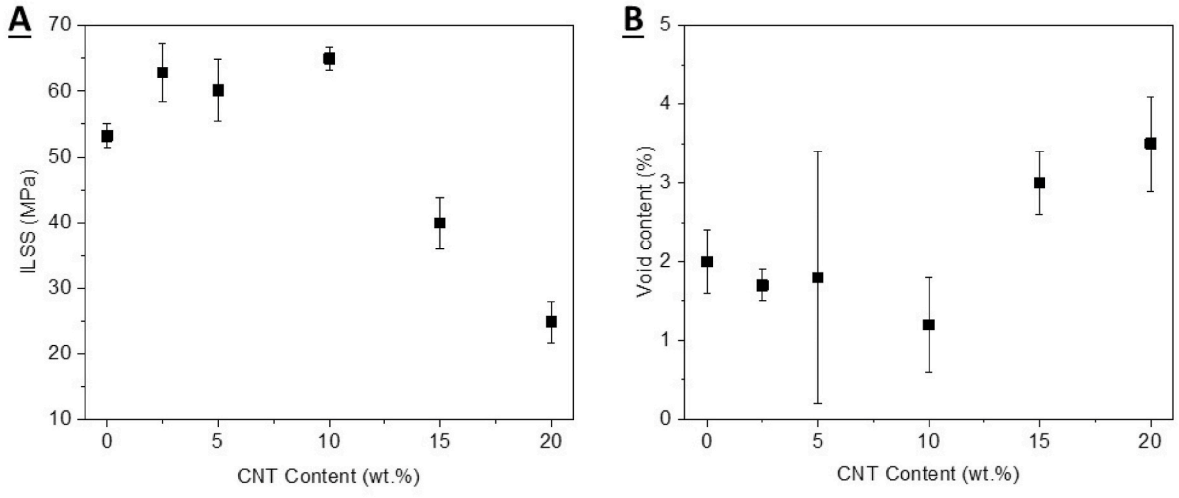


Fig. 4. Interlaminar shear strength of hierarchical composites containing up to 20 wt% CNTs (A) and void content of ILSS hierarchical composites specimens (B).

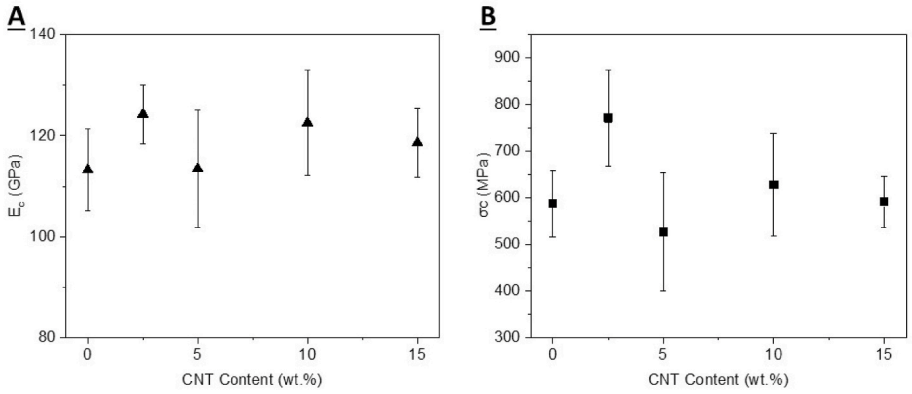


Fig. 5. Absolute compression moduli and standard deviations (A) and absolute compression strength (B) of hierarchical composites containing up to 15 wt% CNTs.

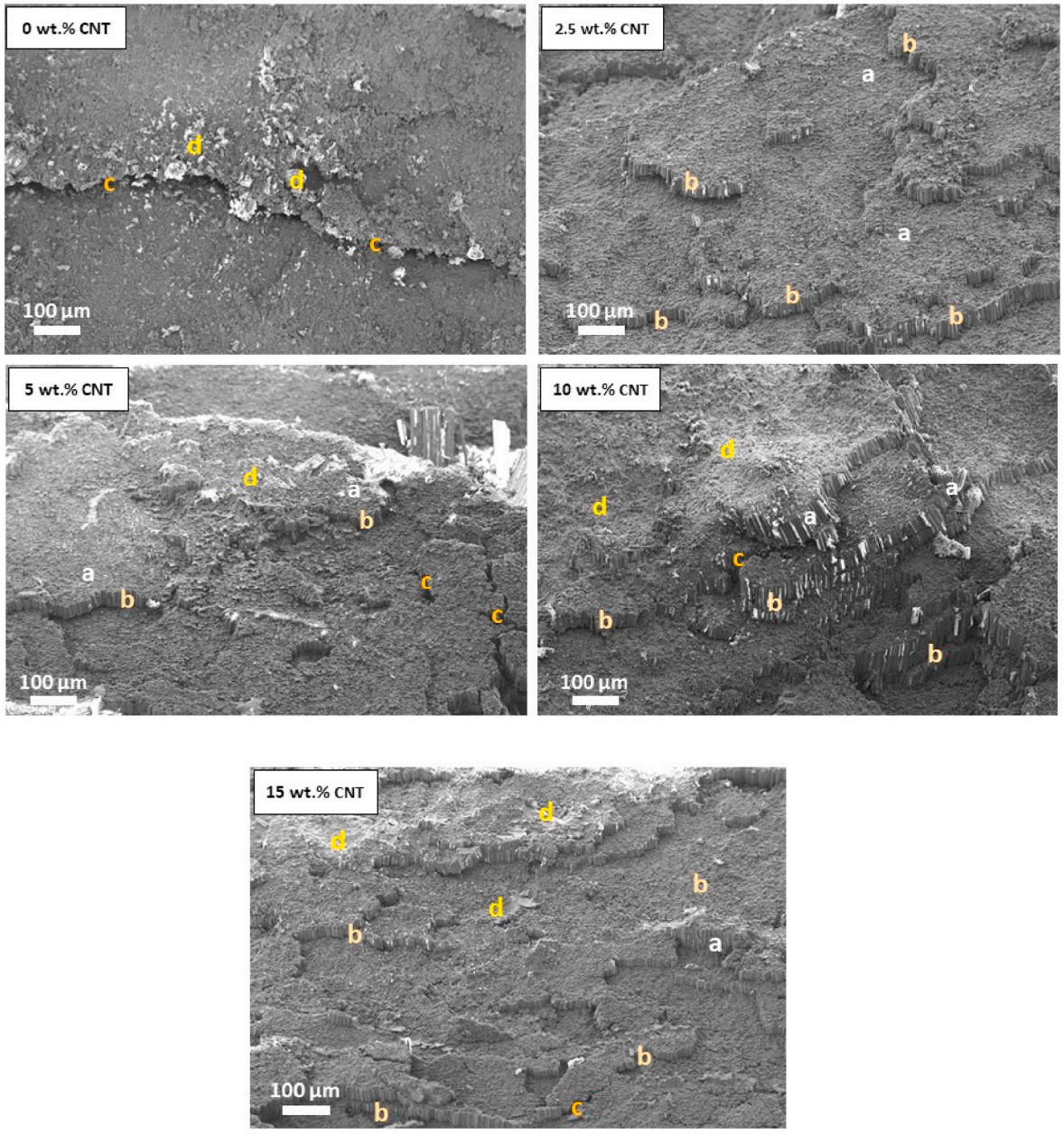


Fig. 6. Selected fractographic SEM images of compression test specimens of the fracture surface (more are included in ESI Fig. S9). Microscopic inspection include (a) microbuckled fibres, (b) terrace of failed fibres, (c) delamination and (d) debris.

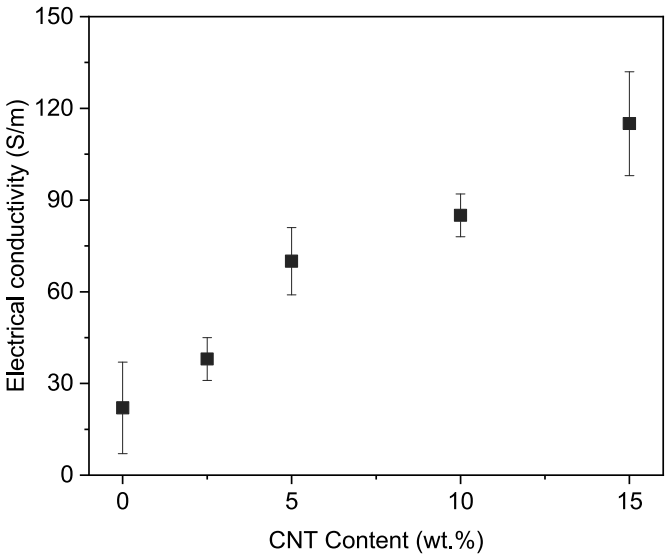


Fig. 7. Through-thickness electrical conductivity of unidirectional hierarchical composites.

resulting in more fibre-fibre contacts. However, the electrical conductivity of the HCs increased significantly with increasing CNT content in the matrix, reaching a maximum (115 ± 17 S/m) at 15 wt% CNTs. The electrical conductivity is twice that of the highest currently reported values for carbon fibre reinforced CNT reinforced composites [24]. These HCs should be appealing for shielding applications and might also be attractive for lightning strike protection in aerospace applications, particularly in mitigating field concentrations associated with metal fastenings; greater through-thickness conductivity may allow more of the in-plane conductivity of the carbon fibres to contribute, reducing the need for addition copper meshes [57].

4. Conclusion

The use of a solid bisphenol-A epoxy resin with a high uncured T_g enabled powder processing to produce both high carbon nanotube content (up to 20 wt%) nanocomposites and hierarchical carbon fibre reinforced nanocomposites. The CNT reinforced resins were manufactured using a simple, scalable melt blending route. An excellent CNT dispersion within the (un)cured resins was observed with an agglomerate size of less than 1 μm. The tensile moduli and strengths of NCs (15 wt% CNT) increased by 32% and 19%, respectively, compared to unreinforced cured epoxy matrix. Unidirectional HCs with an average fibre volume fraction of 57%, a low void fraction (2 ± 1%) and excellent fibre alignment (of about 1° with respect to the tape axis) were prepared using a wet powder impregnation process. The ILSS was highest for HC containing 10 wt% CNTs but decreased with higher CNT loadings. All composites had an average compression modulus around 118 GPa. A significant increase in compression strength was observed for composites containing 2.5 wt% CNTs. The added benefit of the nanocomposite matrix is an increased through-thickness electrical conductivity of 115 S/m for HCs containing 15 wt% CNTs as compared with control composites (22 S/m).

The results show that conventional polymer processing can be used to produce CNT enhanced epoxy resins, which can be further used in powder-based composite prepreg production. The CNT loading can be selected to maximise either interlaminar or compression properties or electrical conductivity without compromising the mechanical properties of the composites. The results show that well-dispersed CNTs within the epoxy matrix enhance ILSS at intermediate CNT loadings and compression strength at low CNT loading, where interfacial failure is avoided; through-thickness electrical conductivity increases linearly with CNT loading. Ultimately, to determine the true potential of these CNT reinforced carbon fibre reinforced epoxy composites as structural composites, inhomogeneities in the laminating process should be reduced further by automation e.g., automated tape laying (ATL), which is a well-established fibre placement technique. ATL eliminates all manual deposition difficulties of UD tapes and produces homogenous large structural composite parts at high speed and greater process control [58]. In contrast to copper meshes laminated onto composite structures, which provide only an electrical conductivity in 2D, these HCs offer enhanced electrical conductivity in all three dimensions. The materials in this study have an electrical conductivity that exceeds that of recently reviewed electrically conducting CFRP [24,59]. The mechanical properties of these HCs are expected to exceed those of matrices augmented with intrinsically conducting polymers or other electrically conductive fillers [59,60]. These HCs offer a practical route to larger scale production of materials with simultaneously enhanced mechanical and functional properties.

Author contribution

N.Y.: Data curation; Formal analysis; Investigation; Methodology; Validation; Visualization; Writing - original draft; **S.J.F.:** Investigation; Formal analysis; **C.B.:** Investigation; Formal analysis; **M.S.P.S.:** Conceptualization, Funding acquisition; Project administration, Supervision; Writing - review & editing; **A.B.:** Conceptualization, Funding acquisition, Resources; Supervision; Writing - review & editing.

Declaration of competing interest

The authors declare that they have no known competing financial interests or personal relationships that could have appeared to influence the work reported in this paper.

Acknowledgements

The authors would like to thank Dstl for funding the research. We would like to thank our students Anto Puljic and Stefan Höfler (both UniVie), Blandine Yverneau and Thomas Bon (exchange students from ICAM), Gaëtan Raimbault (exchange student from Université Haute-Alsace) and Elise Budimirovic (exchange student from Sciences Sorbonne Université) for their help. NY is grateful to the financial support provided by the Institute of Materials Chemistry of the University of Vienna. SF is thankful to the funding from the European Union's Horizon 2020 research and innovation programme under the Marie Sklodowska-Curie grant agreement No 642890.

Appendix A. Supplementary data

Supplementary data to this article can be found online at https://doi.org/10.1016/j.compscitech.2022.109369.

References

[1] A. Brent Strong, Fundamentals of Composites Manufacturing: Materials, Methods and Applications, Society of manufacturing engineers, 2008.
[2] E. Bekyarova, E.T. Thostenson, A. Yu, M.E. Itkis, D. Fakhrutdinov, T.-W. Chou, R. C. Haddon, Functionalized single-walled carbon nanotubes for carbon fiber– epoxy composites, J. Phys. Chem. C 111 (2007) 17865–17871, https://doi.org/10.1021/jp071329a.
[3] A.T. Sunny, P. Vijayan P, R. Adhikari, S. Mathew, S. Thomas, Copper oxide nanoparticles in an epoxy network: microstructure, chain confinement and mechanical behaviour, Phys. Chem. Chem. Phys. 18 (2016) 19655–19667, https://doi.org/10.1039/C6CP02361D.
[4] G. Ungur, J. Hrůza, Influence of copper oxide on the formation of polyurethane nanofibers via electrospinning, Fibers Polym. 16 (2015) 621–628, https://doi.org/10.1007/s12221-015-0621-9.
[5] I.M. El-Nahhal, S.M. Zourab, F.S. Kodeh, M. Selmane, I. Genois, F. Babonneau, Nanostructured copper oxide-cotton fibers: synthesis, characterization, and applications, Int. Nano Lett. 2 (2012) 14, https://doi.org/10.1186/2228-5326-2-14.

[6] L. Fambri, I. Dabrowska, R. Ceccato, A. Pegoretti, Effects of fumed silica and draw ratio on nanocomposite polypropylene fibers, Polymers 9 (2017) 41, https://doi.org/10.3390/polym9020041.

[7] P. Rosso, L. Ye, K. Friedrich, S. Sprenger, A toughened epoxy resin by silica nanoparticle reinforcement, J. Appl. Polym. Sci. 100 (2006) 1849–1855, https://doi.org/10.1002/app.22805.

[8] G. Pandey, E.T. Thostenson, Carbon nanotube-based multifunctional polymer nanocomposites, Polym. Rev. 52 (2012) 355–416, https://doi.org/10.1080/15583724.2012.703747.

[9] H. Qian, E.S. Greenhalgh, M.S. Shaffer, A. Bismarck, Carbon nanotube-based hierarchical composites: a review, J. Mater. Chem. 20 (2010) 4751–4762, https://doi.org/10.1039/c000041h.

[10] P. Rawat, D. Zhu, M.Z. Rahman, F. Barthelat, Structural and mechanical properties of fish scales for the bio-inspired design of flexible body armors: a review, Acta Biomater. 121 (2021) 41–67, https://doi.org/10.1016/j.actbio.2020.12.003.

[11] M. Moniruzzaman, K. Winey, Carbon nanotubes reinforced nylon-6 composite prepared by simple melt-compounding, Macromolecules 39 (2006) 5194–5205, https://doi.org/10.1021/ma035594f.

[12] Z. Han, A. Fina, Thermal conductivity of carbon nanotubes and their polymer nanocomposites: a review, Prog. Polym. Sci. 36 (2011) 914–944, https://doi.org/10.1016/j.progpolymsci.2010.11.004.

[13] P.-C. Ma, N.A. Siddiqui, G. Marom, J.-K. Kim, Dispersion and functionalization of carbon nanotubes for polymer-based nanocomposites: a review, Compos. Part A - Appl. S. 41 (2010) 1345–1367, https://doi.org/10.1016/j.compositesa.2010.07.003.

[14] E.T. Thostenson, T.-W. Chou, Processing-structure-multi-functional property relationship in carbon nanotube/epoxy composites, Carbon 44 (2006) 3022–3029, https://doi.org/10.1016/j.carbon.2006.05.014.

[15] T. Villmow, P. Pötschke, S. Pegel, L. Häussler, B. Kretzschmar, Influence of twin-screw extrusion conditions on the dispersion of multi-walled carbon nanotubes in a poly (lactic acid) matrix, Polymer 49 (2008) 3500–3509, https://doi.org/10.1016/j.polymer.2008.06.010.

[16] D. Poirier, R. Gauvin, R.A. Drew, Structural characterization of a mechanically milled carbon nanotube/aluminum mixture, Compos. Part A - Appl. S. 40 (2009) 1482–1489, https://doi.org/10.1016/j.compositesa.2009.05.025.

[17] M. Šupová, G.S. Martynková, K. Barabaszová, Effect of Nanofillers Dispersion in Polymer Matrices: A Review, Science of Advanced Materials, American Scientific Publishers, 2011.

[18] J.N. Coleman, U. Khan, W.J. Blau, Y.K. Gun'ko, Small but strong: a review of the mechanical properties of carbon nanotube–polymer composites, Carbon 44 (2006) 1624–1652, https://doi.org/10.1016/j.carbon.2006.02.038.

[19] N. Domun, H. Hadavinia, T. Zhang, T. Sainsbury, G.H. Liaghat, S. Vahid, Improving the fracture toughness and the strength of epoxy using nanomaterials – a review of the current status, Nanoscale 7 (2015) 10294–10329, https://doi.org/10.1039/C5NR01354B.

[20] M. Piggott, Matrix Dominated Properties Load Bearing Fibre Composites, Springer, Boston, MA, 2002.

[21] S. Liu, V.S. Chevali, Z. Xu, D. Hui, H. Wang, A review of extending performance of epoxy resins using carbon nanomaterials, Compos. B Eng. 136 (2018) 197–214, https://doi.org/10.1016/j.compositesb.2017.08.020.

[22] Q.-P. Feng, X.-J. Shen, J.-P. Yang, S.-Y. Fu, Y.-W. Mai, K. Friedrich, Synthesis of epoxy composites with high carbon nanotube loading and effects of tubular and wavy morphology on composite strength and modulus, Polymer 52 (2011) 6037–6045, https://doi.org/10.1016/j.polymer.2011.10.049.

[23] T. Yokozeki, Y. Iwahori, S. Ishiwata, K. Enomoto, Mechanical properties of CFRP laminates manufactured from unidirectional prepregs using CSCNT-dispersed epoxy, Compos. Part A - Appl. S. 38 (2007) 2121–2130, https://doi.org/10.1016/j.compositesa.2007.07.002.

[24] T.M. Herceg, M.S. Zainol Abidin, E.S. Greenhalgh, M.S.P. Shaffer, A. Bismarck, Thermosetting hierarchical composites with high carbon nanotube loadings: en route to high performance, Compos. Sci. Technol. 127 (2016) 134–141, https://doi.org/10.1016/j.compscitech.2016.02.015.

[25] M.S.Z. Abidin, T. Herceg, E.S. Greenhalgh, M. Shaffer, A. Bismarck, Enhanced fracture toughness of hierarchical carbon nanotube reinforced carbon fibre epoxy composites with engineered matrix microstructure, Compos. Sci. Technol. 170 (2019) 85–92, https://doi.org/10.1016/j.compscitech.2018.11.017.

[26] K. Ho, S.R. Shamsuddin, S. Riaz, S. Lamorinere, M. Tran, A. Javaid, A. Bismarck, Wet impregnation as route to unidirectional carbon fibre reinforced thermoplastic composites manufacturing, Plast. Rubber Compos. 40 (2011) 100–107, https://doi.org/10.1179/174328911X12988622801098.

[27] S.J. Fisher, M.S. Shaffer, Rapid quantitative mapping of multi-walled carbon nanotube concentration in nanocomposites, Compos. Sci. Technol. 160 (2018) 161–168, https://doi.org/10.1016/j.compscitech.2018.03.010.

[28] C.A. Schneider, W.S. Rasband, K.W. Eliceiri, NIH Image to ImageJ: 25 years of image analysis, Nat. Methods 9 (2012) 671–675, https://doi.org/10.1038/nmeth.2089.

[29] N. Yousefi, M. Jones, A. Bismarck, A. Mautner, Fungal chitin-glucan nanopapers with heavy metal adsorption properties for ultrafiltration of organic solvents and water, Carbohydr. Polym. 253 (2021) 117273, https://doi.org/10.1016/j.carbpol.2020.117273.

[30] N. Yousefi, A.D. Evans, L.T. Harper, H.A. Maples, T. James, A. Bismarck, Solid epoxy resin systems for automated composite manufacturing, Compos. Part A - Appl. S. 142 (2021) 106205, https://doi.org/10.1016/j.compositesa.2020.106205.

[31] Q. Jiang, H. Zhang, D. Rusakov, N. Yousefi, A. Bismarck, Additive manufactured carbon nanotube/epoxy nanocomposites for heavy-duty applications, ACS Appl. Polym. Mater. 3 (2020) 93–97, https://doi.org/10.1021/acsapm.0c01011.

[32] A. Allaoui, N. El Bounia, How carbon nanotubes affect the cure kinetics and glass transition temperature of their epoxy composites? - a review, Express Polym. Lett. 3 (2009) 588–594, https://doi.org/10.3144/expresspolymlett.2009.73.

[33] F.N. Alhabill, T. Andritsch, A.S. Vaughan, The effect of resin/hardener stoichiometry on the electrical properties of silicon nitride/epoxy nanocomposites, in: International Conference on Dielectrics, 2016.

[34] L.S. Cividanes, E.A.N. Simonetti, M.B. Moraes, F.W. Fernandes, G.P. Thim, Influence of carbon nanotubes on epoxy resin cure reaction using different techniques: a comprehensive review, Polym. Eng. Sci. 54 (2014) 2461–2469, https://doi.org/10.1002/pen.23775.

[35] J.-F. Régnier, D. Pothmann-Krings, S. Simar, E. Dony, J.-L. Le Net, J. Beausoleil, Graphistrength© C100 Multiwalled Carbon Nanotubes (MWCNT): thirteen-week inhalation toxicity study in rats with 13- and 52-week recovery periods combined with comet and micronucleus assays, J. Phys. Conf. Ser. 838 (2017), https://doi.org/10.1088/1742-6596/838/1/012030, 012030.

[36] T.M. Herceg, S.H. Yoon, M.S.Z. Abidin, E.S. Greenhalgh, A. Bismarck, M.S. P. Shaffer, Thermosetting nanocomposites with high carbon nanotube loadings processed by a scalable powder based method, Compos. Sci. Technol. 127 (2016) 62–70, https://doi.org/10.1016/j.compscitech.2016.01.017.

[37] L.J. Gibson, Cellular Solids, MRS Bull. 28 (2003) 270–274, https://doi.org/10.1557/mrs2003.79.

[38] H. Krenchel, Fibre Reinforcement; Theoretical and Practical Investigations of the Elasticity and Strength of Fibre-Reinforced Materials, 1964.

[39] J.-P. Salvetat, A.J. Kulik, J.-M. Bonard, G.A.D. Briggs, T. Stöckli, K. Méténier, S. Bonnamy, F. Béguin, N.A. Burnham, L. Forró, Elastic modulus of ordered and disordered multiwalled carbon nanotubes, Adv. Mater. 11 (1999) 161–165, https://doi.org/10.1002/(SICI)1521-4095(199902)11:2<161::AID-ADMA161>3.0.CO;2-J.

[40] J. Gaillard, M. Skove, A.M. Rao, Mechanical properties of chemical vapor deposition-grown multiwalled carbon nanotubes, Appl. Phys. Lett. 86 (2005) 233109, https://doi.org/10.1063/1.1946186.

[41] A.J. Rodriguez, M.E. Guzman, C.-S. Lim, B. Minaie, Mechanical properties of carbon nanofiber/fiber-reinforced hierarchical polymer composites manufactured with multiscale-reinforcement fabrics, Carbon 49 (2011) 937–948, https://doi.org/10.1016/j.carbon.2010.10.057.

[42] Sigrafil, The Enablers - our continuous carbon fiber tows. https://www.sglcarbon.com/pdf/SGL-Broschure-The-Enablers-EN.pdf, 2020. (Accessed 12 May 2021).

[43] S.W. Yurgartis, Measurement of small angle fiber misalignments in continuous fiber composites, Compos. Sci. Technol. 30 (1987) 279–293, https://doi.org/10.1016/0266-3538(87)90016-9.

[44] B. Wang, G. Fang, X. Tan, J. Liang, J. Ge, S. Liu, Investigation on the longitudinal compressive strength of unidirectional carbon fiber/nanoparticles reinforced polymer composites using FFT-based method, Compos. Struct. 247 (2020) 112448, https://doi.org/10.1016/j.compstruct.2020.112448.

[45] J. Cho, J.Y. Chen, I.M. Daniel, Mechanical enhancement of carbon fiber/epoxy composites by graphite nanoplatelet reinforcement, Scripta Mater. 56 (2007) 685–688, https://doi.org/10.1016/j.scriptamat.2006.12.038.

[46] M. Rajanish, N.V. Nanjundaradhya, R.S. Sharma, H.K. Shivananda, A. Hegde, R. S. Darshan, Longitudinal and transverse compressive properties of alumina nanoparticles filled epoxy/unidirectional glass fiber composite laminate under in-plane loading, Mater. Today Proc. 5 (2018) 2921–2927, https://doi.org/10.1016/j.matpr.2018.01.087.

[47] W. Wei, H. Rongjin, H. Chuanjun, Y. Zhao, S. Li, L. Laifeng, Cryogenic performances of T700 and T800 carbon fibre-epoxy laminates, IOP Conf. Ser. Mater. Sci. Eng. 102 (2015), 012016, https://doi.org/10.1088/1757-899x/102/1/012016.

[48] P.K. Mallick, Fiber-reinforced Composites: Materials, Manufacturing, and Design, CRC press, 2007.

[49] E. Greenhalgh, Failure Analysis and Fractography of Polymer Composites, Elsevier, 2009.

[50] A.S. Argon, Fracture of Composites, Treatise on Materials Science & Technology, Elsevier, 1972.

[51] M. Gagné, D. Therriault, Lightning strike protection of composites, Prog. Aero. Sci. 64 (2014) 1–16, https://doi.org/10.1016/j.paerosci.2013.07.002.

[52] S. Pande, A. Chaudhary, D. Patel, B.P. Singh, R.B. Mathur, Mechanical and electrical properties of multiwall carbon nanotube/polycarbonate composites for electrostatic discharge and electromagnetic interference shielding applications, RSC Adv. 4 (2014) 13839–13849, https://doi.org/10.1039/c3ra47387b.

[53] W. Shoukai, D.D.L. Chung, Interlaminar interface in carbon fiber polymer-matrix composites, studied by contact electrical resistivity measurement, Compos. Interfac. 6 (1998) 497–505, https://doi.org/10.1163/156855499X00170.

[54] E.T. Thostenson, J.J. Gangloff Jr., C. Li, J.-H. Byun, Electrical anisotropy in multiscale nanotube/fiber hybrid composites, Appl. Phys. Lett. 95 (2009), 073111, https://doi.org/10.1063/1.3202788.

[55] A. Lonjon, P. Demont, E. Dantras, C. Lacabanne, Electrical conductivity improvement of aeronautical carbon fiber reinforced polyepoxy composites by insertion of carbon nanotubes, J. Non-Cryst. Solids 358 (2012) 1859–1862, https://doi.org/10.1016/j.jnoncrysol.2012.05.038.

[56] L. Du, S.C. Jana, Highly conductive epoxy/graphite composites for bipolar plates in proton exchange membrane fuel cells, J. Power Sources 172 (2007) 734–741, https://doi.org/10.1016/j.jpowsour.2007.05.088.

[57] H. Kawakami, P. Feraboli, Lightning strike damage resistance and tolerance of scarf-repaired mesh-protected carbon fiber composites, Compos. Part A - Appl. S. 42 (2011) 1247–1262, https://doi.org/10.1016/j.compositesa.2011.05.007.

[58] A. Crosky, C. Grant, D. Kelly, X. Legrand, G. Pearce, 4 - fibre placement processes for composites manufacture, in: P. Boisse (Ed.), Advances in Composites Manufacturing and Process Design, Woodhead Publishing, 2015, pp. 79–92.
[59] S. Das, T. Yokozeki, A brief review of modified conductive carbon/glass fibre reinforced composites for structural applications: lightning strike protection, electromagnetic shielding, and strain sensing, Compos. Part C 5 (2021) 100162, https://doi.org/10.1016/j.jcomc.2021.100162.
[60] V. Kumar, T. Yokozeki, C. Karch, A.A. Hassen, C.J. Hershey, S. Kim, J.M. Lindahl, A. Barnes, Y.K. Bandari, V. Kunc, Factors affecting direct lightning strike damage to fiber reinforced composites: a review, Compos. B Eng. 183 (2020) 107688, https://doi.org/10.1016/j.compositesb.2019.107688.